Effect of Baroclinicity on Double-Diffusive Interleaving

BRIAN D. MAY AND DAN E. KELLEY

Department of Oceanography, Dalhousie University, Halifax, Nova Scotia, Canada

(Manuscript received 8 August 1996, in final form 27 February 1997)

ABSTRACT

Although ocean fronts are often baroclinic, existing models of double-diffusive interleaving have ignored such baroclinic effects as velocity shear and horizontal density gradients. To determine the importance of these effects, the authors have formulated a linear instability analysis applicable to baroclinic fronts. Two limiting cases are considered: one for fronts with strong vertical and/or horizontal shear, the other for fronts with weak shear.

In both limits, double-diffusive interleaving can be enhanced or suppressed by baroclinicity. Interleaving motion is enhanced if isopycnals rise toward the fresh side of the front. Conversely, interleaving is suppressed if isopycnals slope downward across the front. A significant result is that the salinity gradient along isopycnals is not a good indicator of interleaving strength.

As an example, the model is applied to a Mediterranean salt lens. The effect of baroclinicity is significant: the predicted growth rates are increased by 35%–90%. The large-scale velocity and hydrographic fields indicate that Meddy Sharon lies somewhere between the high- and low-shear limits. Nevertheless, the model predictions agree reasonably well with the observed interleaving characteristics.

1. Introduction

Inversions are often observed in vertical profiles of temperature and salinity obtained near ocean fronts. The inversions typically have vertical scales of 10 to 100 m. In the presence of horizontal temperature and salinity gradients, they are usually attributed to cross-front ''interleaving'' motions. Theoretical and laboratory studies suggest that interleaving can arise from either of two mechanisms:

- In barotropic thermohaline fronts, unequal mixing of heat and salt can drive double-diffusive interleaving (Stern 1967; Ruddick and Turner 1979).
- In baroclinic fronts, unequal mixing of mass and momentum can drive viscous/diffusive interleaving (McIntyre 1970; Calman 1977).

Ocean observations have provided evidence for double-diffusive interleaving (Horne 1978; Joyce et al. 1978; Ruddick 1992). No conclusive evidence for viscous/diffusive interleaving has been observed to date.

Many ocean fronts are both thermohaline and baroclinic, so they may have both types of interleaving (Ruddick 1992). However, existing theories of double-diffusive interleaving may be inadequate for these fronts because the theories include neither horizontal density gradients nor vertical shear. On the other hand, existing models of viscous/diffusive interleaving may also be invalid because they lack double-diffusive effects. In this paper we address the first of these deficiencies; we develop a new model of double-diffusive interleaving for fronts that are both thermohaline and baroclinic.

First, we review the dynamics and existing theories of double-diffusive interleaving (section 2). Then, we formulate an instability analysis of infinitely wide, baroclinic, thermohaline fronts (section 3). In section 4, we present a new criterion for interleaving and examine its dependence on the isohaline and isopycnal slopes. Then we investigate properties of the fastest-growing modes, separating the analysis into the high- and low-shear cases (section 5). To put the predictions into an oceanographic context, we apply them to a Mediterranean salt lens (section 6). We conclude with a summary of our results and some new questions about the nature of double-diffusive interleaving in ocean fronts (section 7).

2. Dynamics of double-diffusive interleaving

a. Basic mechanism

Double-diffusive interleaving is thought to develop as an instability of thermohaline fronts. In the presence of horizontal gradients, vertically alternating lateral motions cause inversions in the profiles of temperature and salinity (Fig. 1). These fluctuations lead to regions of enhanced double diffusion: salt fingering under warm, salty layers and diffusive convection under layers that are relatively cold and fresh (Turner 1973).

Both forms of double diffusion generate an upgra-

Corresponding author address: Mr. Brian D. May, Department of Oceanography, Dalhousie University, Halifax, NS, B3H 4J1, Canada. E-mail: bmay@phys.ocean.dal.ca

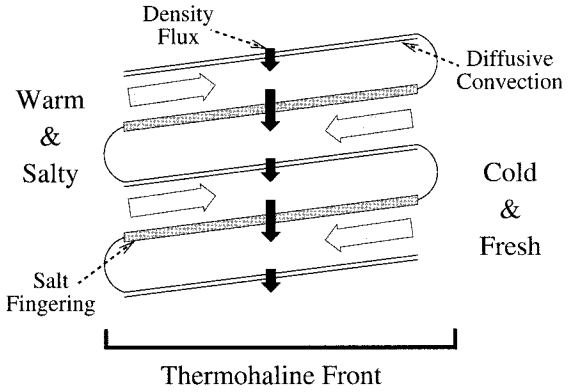

FIG. 1. Side-view illustration of double-diffusive interleaving. The shaded arrows indicate lateral interleaving motions driven by the depth-varying double-diffusive density flux (black vertical arrows). If salt fingering is the dominant form of double diffusion (as shown), warm salty water rises as it crosses the front.

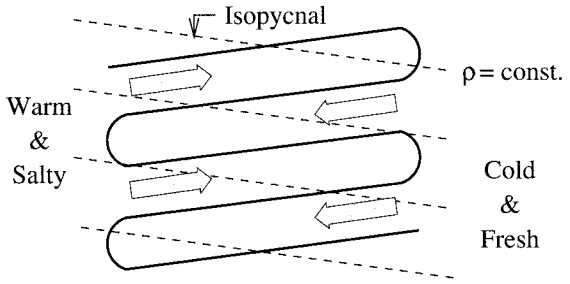

FIG. 2. In this baroclinic front, the isopycnal slope increases the density gradient along the interleaving layers and thus opposes the interleaving motions.

dient (downward) density flux. The convergence of this density flux drives interleaving motions. If the density flux of salt fingering exceeds that of diffusive convection, water in the warm, salty layers becomes less dense and, therefore, rises as it crosses the front. If diffusive convection dominates, water in the cold, fresh layers should rise across the front.

b. Theoretical models of interleaving

Because our work is an extension of existing interleaving models, we start with a brief review of the relevant models. Stern (1967) developed the first model of interleaving, an instability analysis that predicted the initial growth of interleaving. The background front in Stern's model was infinitely wide with constant temperature and salinity gradients throughout. The instabilities predicted were driven by salt fingering; therefore, the layers sloped with warm salty water rising across the front.

A number of models have followed Stern's (1967) approach, making refinements along the way. Toole and Georgi (1981) added friction to Stern's model and predicted an optimum vertical wavelength for the interleaving layers. Niino (1986) extended the model to fronts of arbitrary width. His model matched Toole and Georgi's predictions for wide fronts, but also agreed with the energy-based model of Ruddick and Turner (1979) for narrow fronts.

In Stern's model, salt fingering was assumed to be the only form of double diffusion and a constant diffusivity was used to prescribe the vertical fluxes. Other parameterizations have been considered also. McDougall (1985a) assumed the double-diffusive fluxes to be proportional to the salinity contrast between adjacent layers, rather than the gradient. More recently, Walsh and Ruddick (1995) included a nonconstant diffusivity. In addition, they mapped the analysis to the case driven by diffusive convection, rather than salt fingering. In a model of steady-state interleaving, McDougall (1985b) included both forms of double diffusion.

These models apply to purely thermohaline fronts, that is, fronts with horizontal temperature and salinity gradients, but no horizontal gradients of density. Therefore, the models may not apply to baroclinic fronts, which have nonzero horizontal density gradients as well as vertical shear. One model, by Kuzmina and Rodionov (1992), considered the evolution of interleaving in baroclinic fronts. The model included shear-dependent turbulent mixing in addition to double diffusion and predicted that interleaving strength should decrease with increasing background shear. Unfortunately, the model neglected advection of the background velocity field, which could be important in some fronts. Also neglected was vertical advection of the background salinity field. This approximation is only valid when the density ratio R_ρ is very high, a situation in which double diffusion is unlikely in the first place. These assumptions are not made in the new model presented below.

3. Instability model

a. Introduction

In this paper, we consider two effects of baroclinicity that have not previously been investigated.

- In baroclinic fronts, background shear may distort the interleaving layers. For example, twisting by vertical shear will alter the slope of the layers. Since the slope is dynamically important, shear can be expected to affect the interleaving growth.
- The horizontal density gradient in baroclinic fronts alters the effect of the stratification on interleaving motions. For example, if the isopycnal slope opposes the slope of the interleaving layers, the density gradient along the layers is increased. Therefore, one would expect the interleaving growth to be diminished (Fig. 2).

In the model below, we include vertical shear and a horizontal density gradient. We also include horizontal shear, so the model applies not only to baroclinic fronts but also to sheared barotropic fronts.

We purposefully limit consideration to simple (i.e., geostrophic) fronts in which the gradients of temperature, salinity, and velocity are constant. Ocean fronts are generally more complex. Nevertheless, it is our hope that the results of this model will apply, with the appropriate choice of base-state gradients, to fronts in which the gradients are nonconstant.

b. Base state

The relevant physical quantities are the velocity components (u, v, and w), pressure p, temperature T, salinity S, and density ρ. We use a linear equation of state

$$\frac{1}{\rho_o}\rho = 1 + \beta(S - S_o) - \alpha(T - T_o), \tag{1}$$

where α is the thermal expansion coefficient, β is the contraction coefficient for salinity, and ρ_o is the density at reference temperature T_o and salinity S_o. Following Stern (1967), we separate each of the variables into base-state (overbar) and perturbation (primed) components; for example,

$$u(x, y, z, t) = \bar{u}(x, z) + u'(x, y, z, t). \tag{2}$$

The base state is a steady front and the perturbations are instabilities of the front.

The base state we consider is an infinitely wide front with constant temperature and salinity gradients. The x axis is aligned across the front so that

$$\bar{T}(x, z) = T_o + \bar{T}_x x + \bar{T}_z z \tag{3}$$

$$\bar{S}(x, z) = S_o + \bar{S}_x x + \bar{S}_z z. \tag{4}$$

In our study, the horizontal gradients of temperature and salinity are not assumed to be density compensating, that is, a nonzero horizontal density gradient $\bar{\rho}_x = \rho_o(\beta S_x - \alpha T_x)$ is allowed. The background stratification is assumed to be appropriate for salt fingering ($0 < \beta\bar{S}_z < \alpha\bar{T}_z$); analogy to the diffusive case ($\beta\bar{S}_z < \alpha\bar{T}_z < 0$) is straightforward. The fluid is stably stratified, so $\bar{\rho}_z = \rho_o(\beta\bar{S}_z - \alpha\bar{T}_z) < 0$.

The base state is geostrophic with

$$\bar{u} = 0 \tag{5}$$

$$\bar{v} = v_o + \bar{v}_x x + \bar{v}_z z \tag{6}$$

$$\bar{w} = 0, \tag{7}$$

where the horizontal shear $\bar{v}_x$ and vertical shear $\bar{v}_z$ are assumed to be constant. The vertical shear is related to the horizontal density gradient by the thermal wind relationship

$$f\bar{v}_z = -\frac{g}{\rho_o}\bar{\rho}_x. \tag{8}$$

The horizontal shear is barotropic and, therefore, is independent of the stratification. Note that with constant shear, $\nabla^2\bar{v} = 0$, so friction does not play a role in the base-state dynamics.

c. Perturbation equations of motion

To model the initial growth of interleaving, we consider the evolution of perturbations to the base state. The governing equations for the perturbations are linearized and the fluid is assumed to be Boussinesq, so that

$$\frac{\partial u'}{\partial t} + \underline{\bar{v}\frac{\partial u'}{\partial y}} - fv' + \frac{1}{\rho_o}\frac{\partial p'}{\partial x} - A\frac{\partial^2 u'}{\partial z^2} = 0 \tag{9}$$

$$\frac{\partial v'}{\partial t} + \underline{\bar{v}\frac{\partial v'}{\partial y}} + \underline{u'\bar{v}_x} + \underline{w'\bar{v}_z} + fu' + \frac{1}{\rho_o}\frac{\partial p'}{\partial y} - A\frac{\partial^2 v'}{\partial z^2} = 0 \tag{10}$$

$$\frac{\partial w'}{\partial t} + \underline{\bar{v}\frac{\partial w'}{\partial y}} + \frac{g}{\rho_o}\rho' + \frac{1}{\rho_o}\frac{\partial p'}{\partial z} - A\frac{\partial^2 w'}{\partial z^2} = 0 \tag{11}$$

$$\frac{\partial u'}{\partial x} + \frac{\partial v'}{\partial y} + \frac{\partial w'}{\partial z} = 0 \tag{12}$$

$$\frac{\partial \rho'}{\partial t} + \underline{\bar{v}\frac{\partial \rho'}{\partial y}} + \underline{u'\bar{\rho}_x} + w'\bar{\rho}_z - (1 - \gamma_f)\rho_o\beta K_s\frac{\partial^2 S'}{\partial z^2} = 0 \tag{13}$$

$$\frac{\partial S'}{\partial t} + \underline{\bar{v}\frac{\partial S'}{\partial y}} + u'\bar{S}_x + w'\bar{S}_z - K_s\frac{\partial^2 S'}{\partial z^2} = 0. \tag{14}$$

The underlined terms arise from the background velocity field and horizontal density gradient. These terms have not been included in earlier theories.

An effective viscosity A (typically 10^{-5} to 10^{-3} m^2 s^{-1}) is used to parameterize the momentum fluxes. Assuming salt fingering to be the dominant form of double diffusion, a diffusivity K_s (typically 10^{-6} to 10^{-4} m^2 s^{-1}) is assumed for the vertical salinity flux F_s. The density flux F_ρ is then prescribed by

$$F_\rho = (1 - \gamma_f)\rho_o\beta F_s, \tag{15}$$

where γ_f is a nondimensional flux ratio appropriate for salt fingering (typically 0.5 to 0.9). In practice, the viscosity, diffusivity, and flux ratio are likely to be dependent on parameters such as the density ratio R_ρ (Kelley 1990; Kunze 1994). However, in order to focus on the effects of baroclinicity, we assume these parameters are constant.

Following Stern (1967), we assume that the solution can be expressed as a sum of time-dependent, spatially harmonic modes. This permits the governing differential equations to be reduced to simpler algebraic equations. The assumed waveform is

$$u' = \hat{u}\exp[i(kx + ly + mz) + \lambda t], \tag{16}$$

where $\hat{u}$ is the (complex) amplitude and k, l, and m are the (real) cross-front, alongfront, and vertical wavenumbers, respectively. The growth rate λ may be real or

complex, corresponding to stationary or traveling-wave solutions. We will often describe the interleaving layers in terms of their vertical wavenumber (m), cross-front slope ($-k/m$), and alongfront slope ($-l/m$).

d. Effect of background shear

In baroclinic fronts and sheared barotropic fronts, advection by the background flow (e.g., $\bar{v}\partial u'/\partial y$) can distort the interleaving layers. For the flow given by (5)–(7), the WKB equations describing this distortion (i.e., the evolution of the wavenumbers in time) are

$$\frac{dk}{dt} = -l\bar{v}_x \tag{17}$$

$$\frac{dm}{dt} = -l\bar{v}_z \tag{18}$$

(Kunze 1990). If the alongfront wavenumber l is nonzero, the cross-front and vertical wavenumbers will grow in time, ultimately to infinity.

We concentrate on two limiting cases:

- *High-shear limit.* If the rate of vertical or horizontal shear is large compared to the growth rate λ, the interleaving layers will be tilted out of their unstable range before significant growth can occur, unless the alongfront wavenumber is zero. Therefore, the high-shear modes are derived by setting $l = 0$.
- *Low-shear limit.* If the shear rate is small compared to the growth rate, growth to finite-amplitude can occur before significant tilting takes place. In this case, a nonzero alongfront wavenumber is allowed.

Accordingly, we split the analysis into the high- and low-shear cases. The high-shear limit applies to fronts with strong baroclinic and/or barotropic shear. The low-shear limit applies to fronts in which the shears (and therefore the horizontal density gradient) are weak. Note that the criterion for applying the high- and low-shear limits depends on characteristics of the solution (i.e., the growth rate λ).

e. High-shear limit

The high-shear limit is obtained by setting the alongfront wavenumber to zero. This implies that the interleaving layers do not slope along the front. Using (16) with $l = 0$, the governing equations (9)–(14) become

$$\lambda\hat{u} - f\hat{v} + i\frac{k}{\rho_o}\hat{p} + Am^2\hat{u} = 0 \tag{19}$$

$$\lambda\hat{v} + (f + \bar{v}_x)\hat{u} - \frac{g\bar{\rho}_x}{f\rho_o}\hat{w} + Am^2\hat{v} = 0 \tag{20}$$

$$\lambda\hat{w} + \frac{g}{\rho_o}\hat{\rho} + i\frac{m}{\rho_o}\hat{p} + Am^2\hat{w} = 0 \tag{21}$$

$$ik\hat{u} + im\hat{w} = 0 \tag{22}$$

$$\lambda\hat{\rho} + \bar{\rho}_x\hat{u} + \bar{\rho}_z\hat{w} + (1 - \gamma_f)\rho_o\beta K_s m^2\hat{S} = 0 \tag{23}$$

$$\lambda\hat{S} + \bar{S}_x\hat{u} + \bar{S}_z\hat{w} + K_s m^2\hat{S} = 0, \tag{24}$$

where (8) was used to substitute $\bar{v}_z = -g\bar{\rho}_x/(f\rho_o)$. Note that (22) gives $\hat{w}/\hat{u} = -k/m$, so the cross-front interleaving flow is along the layers. Additionally, there is nonzero perturbation velocity along the front ($\hat{v}$), given by (20).

Eliminating the perturbation amplitudes ($\hat{u}$, $\hat{v}$, $\hat{w}$, $\hat{p}$, $\hat{\rho}$, and $\hat{S}$) from (19)–(24) yields a single equation for the growth rate as a function of the cross-front and vertical wavenumbers. This is

$$\left(1 + \frac{k^2}{m^2}\right)\lambda^4 + \left(1 + \frac{k^2}{m^2}\right)(2A + K_s)m^2\lambda^3 + \left[\left(1 + \frac{k^2}{m^2}\right)(A + 2K_s)Am^4 + f(f + \bar{v}_x) + \frac{g}{\rho_o}\frac{k}{m}\bar{\rho}_x + \frac{g}{\rho_o}\frac{k}{m}\left(\bar{\rho}_x - \frac{k}{m}\bar{\rho}_z\right)\right]\lambda^2$$
$$+ \left[\left(1 + \frac{k^2}{m^2}\right)A^2m^4 + f(f + \bar{v}_x) + \frac{g}{\rho_o}\frac{k}{m}\bar{\rho}_x + (1 + A/K_s)\frac{g}{\rho_o}\frac{k}{m}\left(\bar{\rho}_x - \frac{k}{m}\bar{\rho}_z\right) - (1 - \gamma_f)g\beta\frac{k}{m}\left(\bar{S}_x - \frac{k}{m}\bar{S}_z\right)\right]K_s m^2\lambda$$
$$+ \left[\frac{g}{\rho_o}\frac{k}{m}\left(\bar{\rho}_x - \frac{k}{m}\bar{\rho}_z\right) - (1 - \gamma_f)g\beta\frac{k}{m}\left(\bar{S}_x - \frac{k}{m}\bar{S}_z\right)\right]AK_s m^4 = 0. \tag{25}$$

The terms $\bar{\rho}_x - (k/m)\bar{\rho}_z$ and $\bar{S}_x - (k/m)\bar{S}_z$ are the cross-front gradients of density and salinity along the interleaving layers; they arise from advection of the base-state fields by the perturbation flow. The combination $f(f + \bar{v}_x) + (g/\rho_o)(k/m)\bar{\rho}_x$ arises from planetary rotation and background shear.

For any set of input parameters, the growth-rate polynomial has four roots, each representing an eigenvalue of the dynamical system. The sign of the real part of the growth rate indicates whether the associated solution is growing (positive), decaying (negative), or neutrally stable (zero).

f. Low-shear limit

Before continuing, we derive the corresponding polynomial for the low-shear limit. We assume a priori that the rate of shear deformation is small. Therefore, we allow a nonzero alongfront wavenumber, or equivalently a nonzero alongfront layer slope. When applying the model, care must be taken to ensure that the shear rate is actually small compared to the predicted growth rate.

McDougall (1985a) showed that the alongfront layer slope allows the fastest-growing modes to reach a balance with no alongfront interleaving flow. Setting $v' = 0$ and dropping the shear terms (e.g., $\bar{v}\partial u'/\partial y$), the equations of motion (9)–(14) become

$$\lambda\hat{u} + i\frac{k}{\rho_o}\hat{p} + Am^2\hat{u} = 0 \tag{26}$$

$$(f + \bar{v}_x)\hat{u} - \frac{g\bar{\rho}_x}{f\rho_o}\hat{w} + i\frac{l}{\rho_o}\hat{p} = 0 \tag{27}$$

$$\lambda\hat{w} + \frac{g}{\rho_o}\hat{\rho} + i\frac{m}{\rho_o}\hat{p} + Am^2\hat{w} = 0 \tag{28}$$

$$ik\hat{u} + im\hat{w} = 0 \tag{29}$$

$$\lambda\hat{\rho} + \bar{\rho}_x\hat{u} + \bar{\rho}_z\hat{w} + (1 - \gamma_f)\rho_o\beta K_s m^2\hat{S} = 0 \tag{30}$$

$$\lambda\hat{S} + \bar{S}_x\hat{u} + \bar{S}_z\hat{w} + K_s m^2\hat{S} = 0. \tag{31}$$

Again, $\hat{w}/\hat{u} = -k/m$, so the perturbation flow is along the interleaving layers.

Manipulation of (26) and (28)–(31) yields

$$\left(1 + \frac{k^2}{m^2}\right)\lambda^3 + \left(1 + \frac{k^2}{m^2}\right)(A + K_s)m^2\lambda^2 + \left[\left(1 + \frac{k^2}{m^2}\right)AK_s m^4 + \frac{g}{\rho_o}\frac{k}{m}\left(\bar{\rho}_x - \frac{k}{m}\bar{\rho}_z\right)\right]\lambda + \left[\frac{g}{\rho_o}\frac{k}{m}\left(\bar{\rho}_x - \frac{k}{m}\bar{\rho}_z\right) - (1 - \gamma_f)g\beta\frac{k}{m}\left(\bar{S}_x - \frac{k}{m}\bar{S}_z\right)\right]K_s m^2 = 0. \tag{32}$$

In this case, the interleaving dynamics are independent of the *y*-momentum equation, so the growth-rate polynomial is a cubic. With $\bar{\rho}_x = 0$, (32) reduces to the model of Toole and Georgi (1981). Our low-shear limit is an extension of their model to baroclinic fronts.

Equation (27) prescribes the alongfront slope required to maintain $v' = 0$. Combining (26)–(27) and (29), we find that the slope is

$$\frac{l}{m} = \left(f + \bar{v}_x + \frac{k}{m}\frac{g\bar{\rho}_x}{f\rho_o}\right)\frac{k/m}{\lambda + Am^2}. \tag{33}$$

The predicted alongfront slope can be much larger than the cross-front slope, indicating that the interleaving motions are strongly affected by rotation.

The WKB equations (17)–(18) show that the layers will be distorted by background shear if they slope along the front. The low-shear polynomial (32) is only valid if the rate of this distortion is small compared to the growth rate (λ).

- The rate at which the wave vector will be rotated by horizontal (i.e., barotropic) shear is $|\bar{v}_x|$. Therefore, application of the low-shear limit requires

$$|\bar{v}_x| \ll \lambda. \tag{34}$$

- The rate of distortion by vertical (i.e., baroclinic) shear is $|(l/m)\bar{v}_z|$. Application of the low-shear limit requires

$$\left|\frac{l}{m}\bar{v}_z\right| = \left|\frac{l}{m}\frac{g\bar{\rho}_x}{f\rho_o}\right| \ll \lambda. \tag{35}$$

Both requirements depend on the solutions (i.e., l/m and λ), so they must be checked after solving the growth-rate polynomial. In section 5, we investigate fastest-growing modes and give some guidelines as to when the low-shear limit applies.

4. Criterion for growth of double-diffusive interleaving

a. Modes of instability

To expose instabilities of the front, we consider only solutions with positive λ. As Stern (1967) noted, we are guaranteed at least one positive root if the term independent of λ in the growth-rate polynomial [(25) or (32)] is negative. This is the criterion for double-diffusive interleaving.

In baroclinic fronts, there are additional possibilities for growth. If the λ coefficient is negative, there are generally two roots of the growth-rate polynomial with positive real parts. These roots correspond to the viscous/diffusive instability predicted by McIntyre (1970). A third instability, ''slant-wise convection'' (Emanuel 1994), can occur if the λ^2 coefficient is negative. This form of instability cannot occur unless a modified Richardson number $(N^2/\bar{v}_z^2)(1 + \bar{v}_x/f)$ is less than one.

b. Criterion for double-diffusive interleaving

The focus of our investigation is double-diffusive interleaving. Dividing (25) by $gAK_s m^4$ and (32) by $gK_s m^2$, we see that the term independent of λ is negative when

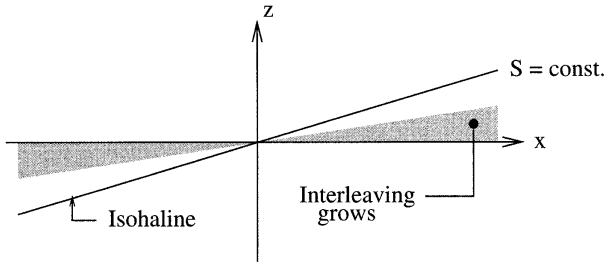

FIG. 3. Range of interleaving slopes (shaded) when the isopycnals are flat (i.e., $\bar{\rho}_x = 0$).

$$\frac{1}{\rho_o}\frac{k}{m}\left(\bar{\rho}_x - \frac{k}{m}\bar{\rho}_z\right) - (1 - \gamma_f)\beta\frac{k}{m}\left(\bar{S}_x - \frac{k}{m}\bar{S}_z\right) < 0. \tag{36}$$

This is the criterion for double-diffusive interleaving. It holds in both the high- and low-shear limits.

The first term in (36) is negative if $k/m \in (0, \bar{\rho}_x/\bar{\rho}_z)$, that is, if the layer slope $(-k/m)$ lies between zero and the isopycnal slope $(-\bar{\rho}_x/\bar{\rho}_z)$. This range of slopes defines the baroclinic wedge of instability; when the layer slope is in this range, baroclinicity enhances the interleaving motion. With $\bar{S}_z > 0$, the second term in (36) is negative if $k/m \in (0, \bar{S}_x/\bar{S}_z)$, that is, if the layer slope $(-k/m)$ lies between zero and the isohaline slope $(-\bar{S}_x/\bar{S}_z)$. We refer to this range of slopes as the double-diffusive wedge of instability; in this range, double diffusion provides the driving mechanism for interleaving motions.

The instability criterion (36) depends on both the density and salinity distributions. It is satisfied if

$$\frac{k}{m} \in \left(0, \frac{(1 - \gamma_f)\beta\bar{S}_x - \bar{\rho}_x/\rho_o}{(1 - \gamma_f)\beta\bar{S}_z - \bar{\rho}_z/\rho_o}\right). \tag{37}$$

In this range, the combined effects of density advection and diffusion are destabilizing. The maximum unstable interleaving slope is the cross-front slope along which the ratio of the density and salinity gradients $(\Delta\rho/\rho_o)/(\beta\Delta S)$ equals the flux ratio $(1 - \gamma_f)$.

Introducing the nondimensional quantity $\epsilon_z \equiv -(1 - \gamma_f)\beta\bar{S}_z/(\bar{\rho}_z/\rho_o) = (1 - \gamma_f)/(R_\rho - 1)$ (Toole and Georgi 1981), we rewrite (37) as

$$\frac{k}{m} \in \left(0, \frac{\epsilon_z\bar{S}_x/\bar{S}_z + \bar{\rho}_x/\bar{\rho}_z}{\epsilon_z + 1}\right). \tag{38}$$

This shows that the maximum layer slope is a weighted average of the isohaline and isopycnal slopes. In the ocean, they are typically 10^{-4} to 10^{-2}, so the interleaving slopes are roughly this size. The weight ϵ_z is positive under the assumption $\bar{S}_z > 0$ and is typically in the range 0.2 to 1.

c. Flat isopycnals

When the isopycnals are flat (i.e., $\bar{\rho}_x = 0$), interpretation of (38) is straightforward. The maximum interleaving slope always lies between zero and the isohaline slope, so the interleaving layers slope upward into fresher water (Fig. 3). Due to the stratification, the limit for growth is less than the isohaline slope by the factor $\epsilon_z/(\epsilon_z + 1)$.

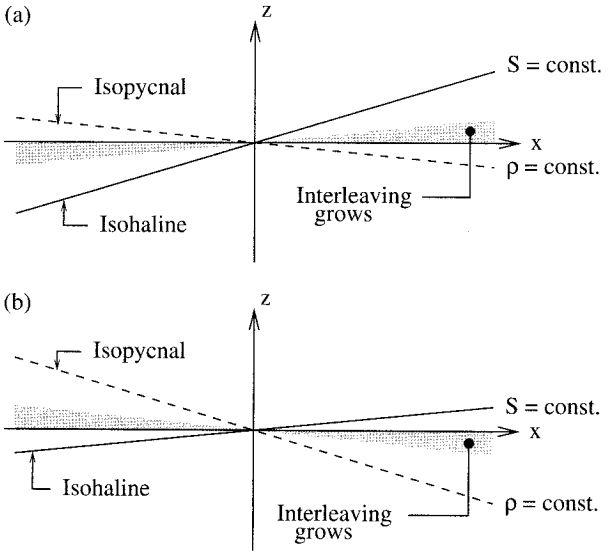

FIG. 4. Range of interleaving slopes (shaded) when the isopycnal and isohaline slopes are of opposite sign [i.e., $(\bar{\rho}_x/\bar{\rho}_z)/(\bar{S}_x/\bar{S}_z) < 0$]: (a) small isopycnal slope and (b) large isopycnal slope.

d. Opposing isopycnal and isohaline slopes

If the isopycnal slope opposes the isohaline slope [i.e., $(\bar{\rho}_x/\bar{\rho}_z)/(\bar{S}_x/\bar{S}_z) < 0$], the double-diffusive and baroclinic wedges of instability do not overlap (Fig. 4). The range of interleaving slopes depends on the relative magnitudes of $\bar{\rho}_x$ and $\bar{S}_x$.

- If the horizontal salinity gradient dominates [i.e., $(1 - \gamma_f)\beta|\bar{S}_x| > |\bar{\rho}_x|/\rho_o$], the maximum interleaving slope lies between zero and the isohaline slope (Fig. 4a). Therefore, the instabilities lie in the double-diffusive wedge of instability.
- If, on the other hand, the density gradient dominates [i.e., $|\bar{\rho}_x|/\rho_o > (1 - \gamma_f)\beta|\bar{S}_x|$], the maximum interleaving slope lies between zero and the isopycnal slope (Fig. 4b). The instabilities lie in the baroclinic wedge of instability.

The second case is a form of baroclinic instability that has not been predicted before. Unlike McIntyre's (1970) viscous instability, the instability criterion does not depend on the relative rates of viscosity and diffusion. Instead, it depends on the inability of double-diffusive fluxes to completely remove fluctuations in the density field.

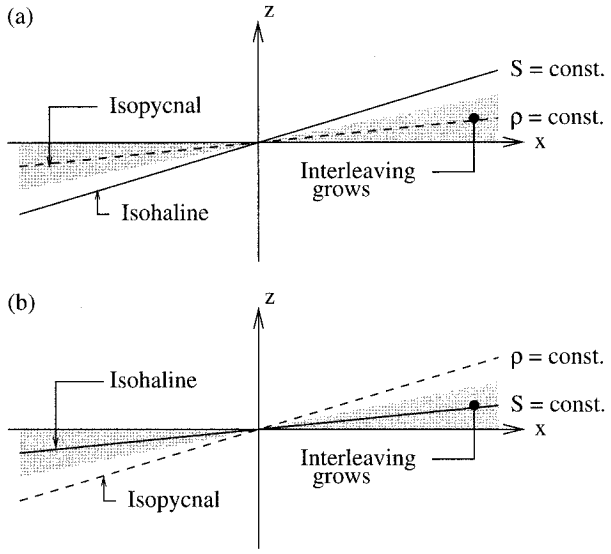

FIG. 5. Range of interleaving slopes (shaded) when the isopycnal and isohaline slopes have the same sign [i.e., $(\bar{\rho}_x/\bar{\rho}_z)/(\bar{S}_x/\bar{S}_z) > 0$]: (a) small isopycnal slope and (b) large isopycnal slope.

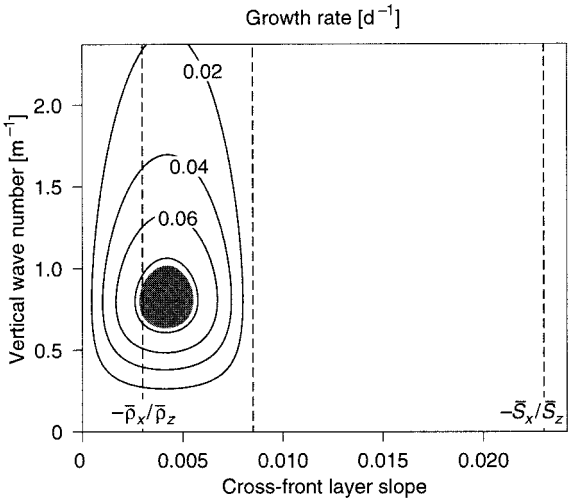

FIG. 6. Contour plot of the high-shear growth rate [λ in (25)] as a function of the cross-front layer slope ($-k/m$) and vertical wavenumber (m). The input parameters were taken from Table 1. The isopycnal slope ($-\bar{\rho}_x/\bar{\rho}_z$), isohaline slope ($-\bar{S}_x/\bar{S}_z$), and maximum unstable slope [given by (37)] are indicated. The shaded area illustrates the range in which λ is greater than 90% of its maximum value (e-folding period of 11 days).

e. Isopycnal and isohaline slopes of same sign

If the isopycnal and isohaline slopes have the same sign [i.e., $(\bar{\rho}_x/\bar{\rho}_z)/(\bar{S}_x/\bar{S}_z) > 0$], the double-diffusive and baroclinic wedges of instability overlap (Fig. 5). Again, the range of interleaving slopes depends on the relative magnitudes of $\bar{\rho}_x$ and $\bar{S}_x$.

- If the isohaline slope exceeds the isopycnal slope (i.e., $|\bar{S}_x/\bar{S}_z| > |\bar{\rho}_x/\bar{\rho}_z|$); the limit for growing instabilities extends beyond the slope of the isopycnals (Fig. 5a).
- If, on the other hand, the isohalines slope less steeply than the isopycnals (i.e., $|\bar{S}_x/\bar{S}_z| < |\bar{\rho}_x/\bar{\rho}_z|$), the limit for growing instabilities extends beyond the isohaline slope (Fig. 5b).

Depending on the slope of the interleaving layers relative to the isopycnal and isohaline surfaces, interleaving motions may be driven by double diffusion, baroclinicity, or both.

5. Fastest-growing modes

a. High-shear limit

In the high-shear limit, (25) is used to calculate the growth rate (λ). For a given base state and flux parameterization, the growth rate is a function of the cross-front slope ($-k/m$) and vertical wavenumber (m) (Fig. 6). It is positive within the range of slopes prescribed by (37) for all values of vertical wavenumber.

The values of k and m that maximize λ are of particular interest. These are the properties one might expect to find when a set of random initial perturbations has grown to finite amplitude. In the high-shear limit, the cross-front slope of the fastest-growing mode is roughly half the maximum unstable slope. The vertical wavelength of the fastest-growing mode is roughly the Ekman scale $2\pi(A/|f|)^{1/2}$.

To illustrate the effect of baroclinicity on the fastest-growing solutions, the optimum cross-front slope, vertical wavenumber, and growth rate have been plotted as functions of isopycnal slope (Fig. 7). The cross-front slope increases linearly with isopycnal slope and the growth rate has a quadratic dependence. Interleaving is enhanced if the isopycnal slope is positive (i.e., if the isopycnals rise toward the fresh side of the front). Note that the slope and growth rate of the fastest-growing mode go to zero when $(1 - \gamma_f)\beta\bar{S}_x = \bar{\rho}_x/\rho_o$. The optimum vertical wavelength is affected little by baroclinicity.

Numerical maximization of the growth rate in (25) is straightforward. However, we must make a number of approximations in the growth-rate polynomial to obtain analytical expressions for the fastest-growing mode.

- In the ocean, the isohaline and isopycnal slopes are usually much smaller than one, so the layer slopes are also very small. We can approximate $1 + k^2/m^2 \approx 1$.
- When the slope of the interleaving layers is small compared to the frequency ratio f/N, the polynomial can be simplified even further. We will show that $\lambda \ll K_s m^2$ and $\lambda \ll Am^2$ in this case.

Because these approximations depend on characteristics of the solutions, it is necessary to verify a posteriori that they hold.

With $1 + k^2/m^2 \approx 1$, $\lambda \ll K_s m^2$, and $\lambda \ll Am^2$, (25) reduces to the much simpler relation

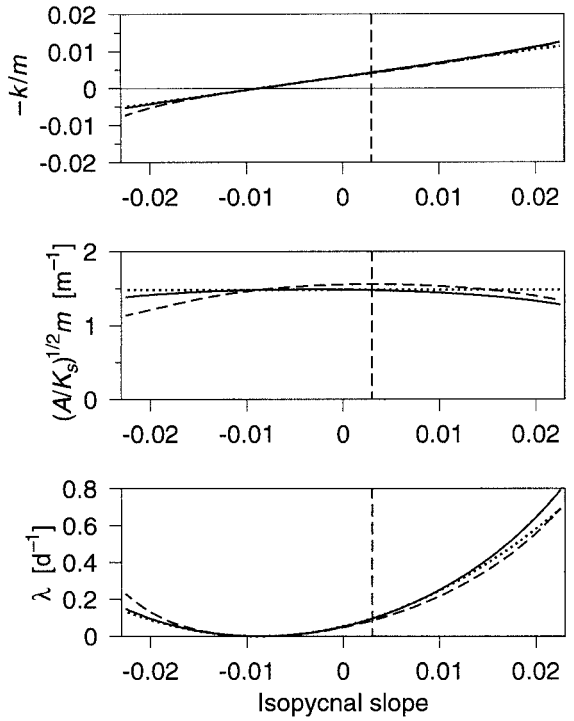

FIG. 7. Optimum cross-front slope ($-k/m$), vertical wavenumber (m), and growth rate (λ) for the high-shear limit vs isopycnal slope. The input parameters were taken from Table 1. The observed isopycnal slope is indicated. To illustrate dependence on the Prandtl number (A/K_s), the calculations were performed with $A = K_s$ (solid lines) and $A = 10K_s$ (dashed lines), holding K_s constant. The dotted lines indicate approximate solutions given by (40)–(42). The vertical wavenumber axis was scaled to take into account the theoretical Prandtl-number dependence.

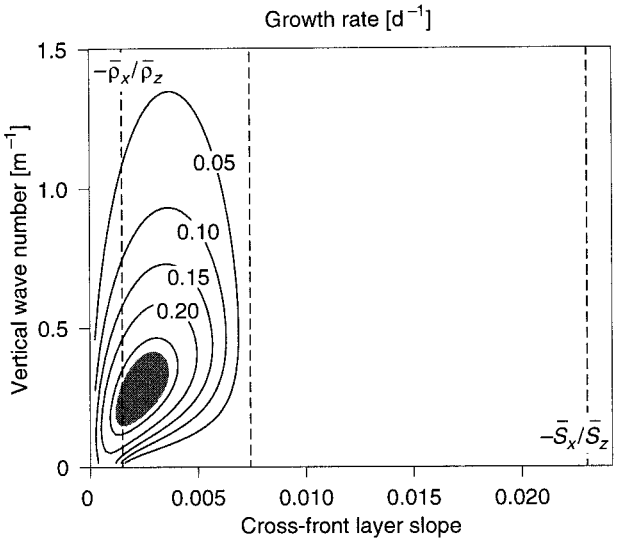

FIG. 8. As in Fig. 6 but for the low-shear limit [λ given by (32)]. The input parameters were taken from Table 1, except the horizontal density gradient, which was reduced by 50% to ensure satisfaction of (35) near the maximum. The e-folding period of the fastest-growing mode is roughly 3 days.

$$[A^2m^4 + f(f + \bar{v}_x)]\lambda + \left[\frac{g}{\rho_o}\frac{k}{m}\left(\bar{\rho}_x - \frac{k}{m}\bar{\rho}_z\right) - (1 - \gamma_f)g\beta\frac{k}{m}\left(\bar{S}_x - \frac{k}{m}\bar{S}_z\right)\right]Am^2 = 0. \quad (39)$$

Maximizing λ with respect to k and m gives

$$\frac{k}{m} = \frac{g}{2N^2}\frac{(1 - \gamma_f)\beta\bar{S}_x - \bar{\rho}_x/\rho_o}{(1 + \epsilon_z)} \quad (40)$$

$$m^2 = \frac{|f|}{A}(1 + \bar{v}_x/f)^{1/2} \quad (41)$$

$$\lambda = \frac{g^2}{8|f|N^2}\frac{[(1 - \gamma_f)\beta\bar{S}_x - \bar{\rho}_x/\rho_o]^2}{(1 + \epsilon_z)(1 + \bar{v}_x/f)^{1/2}}, \quad (42)$$

where $N^2 = -g\bar{\rho}_z/\rho_o$ and $\varepsilon_z = -(1 - \gamma_f)\beta\bar{S}_z/(\bar{\rho}_z/\rho_o) = (1 - \gamma_f)/(R_\rho - 1)$.

It is easily shown that $\lambda \ll K_sm^2$ and $\lambda \ll Am^2$, provided $k^2/m^2 \ll f^2/N^2$ and $k^2/m^2 \ll (A/K_s)f^2/N^2$. In the example, $f/N \approx 0.03$, so these approximations are valid over most of the illustrated range (Fig. 7). The approximate solutions (40)–(42) are quite close to the numerical results.

b. Low-shear limit

In the low-shear limit, the growth of interleaving is prescribed by (32). As in the high-shear limit, the rate of growth is positive within the range of cross-front slopes specified by (37) (Fig. 8). Compared to the high-shear case, the maximum is shifted to smaller cross-front slope and vertical wavenumber. The optimum growth rate is increased.

The dependence of the fastest-growing mode on the isopycnal slope is illustrated in Fig. 9. At low Prandtl number ($A = K_s$), the cross-front interleaving slope increases with isopycnal slope and the vertical wavenumber is roughly constant. The dependence at higher Prandtl number ($A = 10K_s$) is significantly different. The cross-front slope is roughly constant and the vertical wavenumber decreases as the isopycnal slope is increased. In both cases, the growth rate increases with increasing isopycnal slope. This implies that interleaving is enhanced if the isopycnals slope upward toward the fresh side of the front.

In Fig. 9, and we only plotted solutions that grow faster than the rate of distortion by vertical shear [i.e., $\lambda > |(l/m)\bar{v}_z|$]. The figure shows that the low-shear limit is restricted to fronts with small isopycnal slope. The observed isopycnal slope is near the upper bound for application of the low-shear polynomial.

As in the high-shear limit, the growth-rate polynomial (32) must be approximated to obtain analytical expressions for the fastest-growing mode.

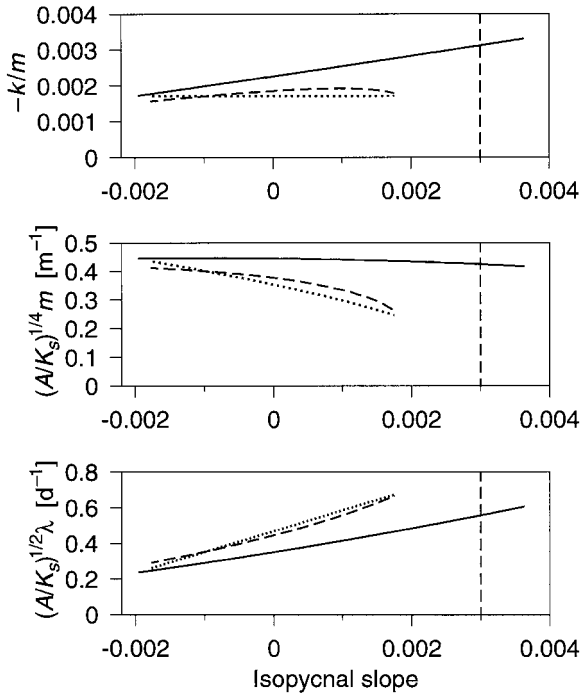

FIG. 9. As in Fig. 7 but for the low-shear limit [λ given by (32)]. The observed isopycnal slope is indicated. Only solutions satisfying the low-shear criterion (35) are plotted. Fastest-growing modes were calculated with $A = K_s$ (solid lines) and $A = 10K_s$ (dashed lines), holding K_s constant. The dotted lines indicate approximate solutions given by (44)–(46).

- Assuming the isohaline and isopycnal slopes to be much smaller than one, we set $1 + k^2/m^2 \approx 1$.
- Following Toole and Georgi (1981) and McDougall (1985a), we consider a limit in which the Prandtl number is large (i.e., $A/K_s \gg 1$). We will show that $\lambda \ll Am^2$ in this case.

The Prandtl number is not necessarily large in the ocean ($A/K_s \approx 4$ in Table 1). Nevertheless, the second approximation is useful in that it allows us to derive analytical solutions and to compare these solutions with earlier theories.

With $1 + k^2/m^2 \approx 1$ and $\lambda \ll Am^2$, the low-shear polynomial (32) becomes

$$Am^2\lambda^2 + \left[AK_sm^4 - \frac{g}{\rho_o}\frac{k}{m}\left(\bar{\rho}_x - \frac{k}{m}\bar{\rho}_z\right)\right]\lambda + \left[\frac{g}{\rho_o}\frac{k}{m}\left(\bar{\rho}_x - \frac{k}{m}\bar{\rho}_z\right) - (1-\gamma_f)g\beta\frac{k}{m}\left(\bar{S}_x - \frac{k}{m}\bar{S}_z\right)\right]K_sm^2 = 0. \quad (43)$$

Despite these simplifications, maximization of (43) remains a challenge. Keeping in mind that the low-shear limit is applicable at small isopycnal slopes, we tackle the problem as a perturbation analysis, using the ratio $(\bar{\rho}_x/\rho_o)/(\beta\bar{S}_x)$ as an ordering parameter. The zeroth-order solution ($\bar{\rho}_x = 0$) matches existing theories, which do not include baroclinicity (Toole and Georgi 1981; McDougall 1985a).

TABLE 1. Base-state properties for Meddy Sharon.

Quantity	Value
g	9.8 m s^{-2}
f	7.7×10^{-5} s^{-1}
β	7.5×10^{-4} psu^{-1}
$\bar{S}_x$	$-2.9(\pm0.4) \times 10^{-5}$ psu m^{-1}
$\bar{S}_z$	$1.23(\pm0.03) \times 10^{-3}$ psu m^{-1}
ρ_o	1032 kg m^{-3}
$\bar{\rho}_x$	$2.3(\pm1.0) \times 10^{-6}$ kg m^{-4}
$\bar{\rho}_z$	$-7.52(\pm0.07) \times 10^{-4}$ kg m^{-4}
K_s	1.2 to 7.5 ($\times10^{-5}$ m^2 s^{-1})
A	0.3 to 4.0 ($\times10^{-4}$ m^2 s^{-1})
γ_f	0.7($\pm$0.1)
ζ	$0.6(\pm0.2) \times 10^{-5}$ s^{-1})
η	$1.1(\pm0.4) \times 10^{-5}$ s^{-1}

To determine the first-order effect of baroclinicity, we maximize λ with respect to k and m, retaining terms of order $(\bar{\rho}_x/\rho_o)/(\beta\bar{S}_x)$. This yields

$$\frac{k}{m} = \frac{g}{2N^2}\frac{(1-\gamma_f)\beta\bar{S}_x}{1+\epsilon_z+(1+\epsilon_z)^{1/2}} \quad (44)$$

$$m^2 = \frac{g}{2N(AK_s)^{1/2}}\left|\frac{(1-\gamma_f)\beta\bar{S}_x}{1+\epsilon_z+(1+\epsilon_z)^{1/2}} + \frac{\bar{\rho}_x}{\rho_o}\right| \quad (45)$$

$$\lambda = \frac{g}{2N}\left(\frac{K_s}{A}\right)^{1/2}\left|\frac{(1-\gamma_f)\beta\bar{S}_x}{1+(1+\epsilon_z)^{1/2}} - \frac{\bar{\rho}_x}{\rho_o}\right|. \quad (46)$$

From these solutions, it is easy to show that $\lambda \ll Am^2$, provided $A/K_s \gg 1$. Comparison of (44)–(46) with the numerical results (at high Prandtl number) yields good agreement (Fig. 9).

Using the approximate solutions (44)–(46) we can derive rough guidelines for determining when the low-shear limit should apply. From (34), the requirement for the horizontal (i.e., barotropic) shear is

$$|\bar{v}_x| \ll \frac{g}{2N}\left(\frac{K_s}{A}\right)^{1/2}\left|\frac{(1-\gamma_f)\beta\bar{S}_x}{1+(1+\epsilon_z)^{1/2}} - \frac{\bar{\rho}_x}{\rho_o}\right|. \quad (47)$$

This condition should be satisfied in order to apply the low-shear limit.

The required alongfront slope is given by (33) and is roughly

$$\left|\frac{l}{m}\right| \approx \frac{|f|}{N}\left(\frac{K_s}{A}\right)^{1/2}. \quad (48)$$

Therefore, the requirement on the vertical (i.e., baroclinic) shear (35) becomes

$$\left|\frac{\bar{\rho}_x}{\rho_o}\right| \ll \frac{1}{2}\left|\frac{(1-\gamma_f)\beta\bar{S}_x}{1+(1+\epsilon_z)^{1/2}}\right|. \quad (49)$$

Application of the low-shear limit is restricted to weakly baroclinic fronts, that is, fronts in which the horizontal density gradient $\overline{\rho}_x/\rho_o$ is much smaller than the horizontal salinity gradient $\beta\overline{S}_x$.

6. Application to Meddy Sharon

a. Overview

In order to establish an oceanographic context for our model, we applied it to a previously studied front in which double-diffusive interleaving has been observed. Meddy Sharon, a lens of Mediterranean Water observed in the eastern North Atlantic (Armi et al. 1989), is a good test site for several reasons. During the period of observation, its heat and salt characteristics were gradually eroded away by lateral interleaving (Hebert et al. 1990). The doming of isopycnals associated with the meddy indicates that it caused a density front as well as a front in temperature and salinity. We should note that the meddy example may not represent a typical ocean regime because it was a region of particularly high gradients and strong shears. However, it does make a good test case for our theory.

b. Base state

The lower part of the meddy was stratified appropriately for salt fingering and has been most intensively studied, so we focus on that region. The quantities used in this analysis are listed in Table 1.

The seven ''tow-yo'' profiles considered by Ruddick (1992) were reanalyzed to estimate the horizontal and vertical gradients of salinity and density. The salt diffusivity K_s was calculated following Ruddick and Hebert (1988), but the uncertainty in the observed vertical wavelength was included in the calculation. We used microstructure measurements (Oakey 1988) together with the observed velocity field (Armi et al. 1989) to estimate a vertical eddy viscosity appropriate to the scales of interest ($A \approx \varepsilon/\overline{v}_z^2$). The value obtained, 0.3 to 4.0 ($\times 10^{-4}$ m^2 s^{-1}), is consistent with other estimates of viscosity in double-diffusive systems (Schmitt et al. 1986; Padman 1994) and with Ruddick et al. (1989), who suggested that the Prandtl number should be $O(1)$. Our estimate of the salt-finger flux ratio (γ_f) is taken from McDougall and Ruddick (1992), who reviewed published estimates and concluded that the most probable range for oceanic salt fingering is 0.6 to 0.8.

Estimates of vorticity ζ and strain η were obtained from Hebert (1988). Because the meddy was a circular vortex, we cannot simply substitute a single value for $\overline{v}_x$ in our equations. Where $\overline{v}_x$ appears in the form $1 + \overline{v}_x/f$, the vorticity is the relevant quantity (i.e., we substitute $1 + \zeta/f$). In (34) and (47), however, the strain dictates the rate of distortion, so we substitute $\overline{v}_x = \eta$.

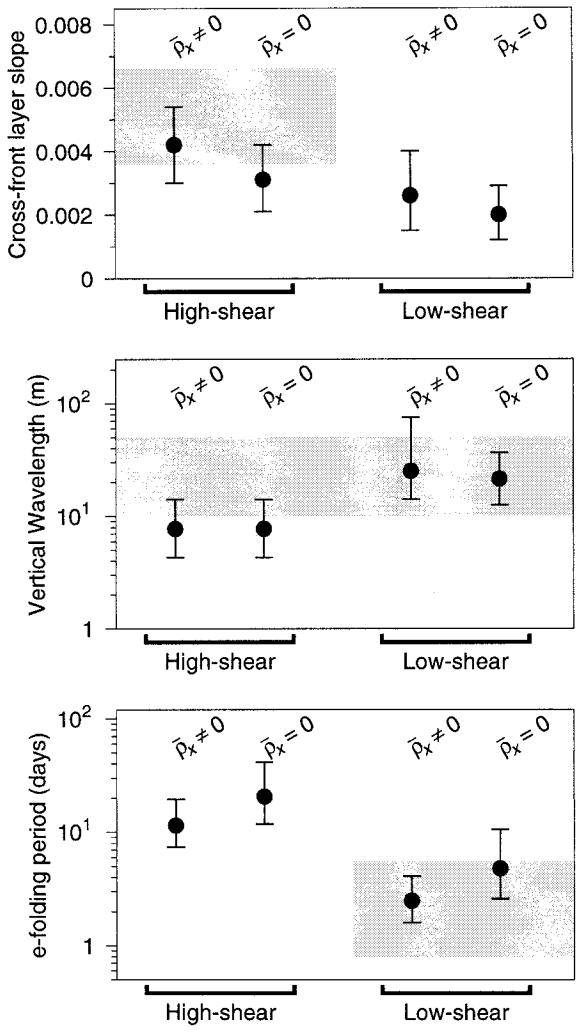

FIG. 10. Cross-front layer slope, vertical wavelength, and *e*-folding period of the fastest-growing modes, for the high- and low-shear limits. The calculations were made using the observed cross-front density gradient ($\overline{\rho}_x \neq 0$) and, for comparison, setting the cross-front density gradient to zero ($\overline{\rho}_x = 0$). In the first two panels, the shaded regions indicate the observed slope and wavelength. In the final panel, the rate of distortion by background shear is shaded.

c. Model predictions

It is not clear a priori whether the high- or low-shear limit applies to Meddy Sharon. Therefore, we estimate the optimum cross-front slope ($-k/m$), vertical wavelength ($2\pi/m$), and *e*-folding period ($1/\lambda$) for both cases (Fig. 10). To illustrate the effect of baroclinicity, the calculations were performed using the observed horizontal density gradient ($\overline{\rho}_x \neq 0$) and, for comparison, setting the horizontal density gradient to zero ($\overline{\rho}_x = 0$).

In the high-shear limit, numerical maximization of (25) gives a predicted cross-front slope of 4×10^{-3}, vertical wavelength of 8 m, and *e*-folding period of 11 days (Fig. 10). The predicted layer slope roughly matches the observed isopycnal slope of $3(\pm 1) \times 10^{-3}$. This

suggests that the layers should slope upward relative to geopotential surfaces, but should not necessarily slope relative to the isopycnals. Including the horizontal density gradient increased the predictions of cross-front slope and growth rate by 35% and 45%, respectively. However, the predicted vertical wavelength was unchanged.

In the low-shear limit, maximizing (32) gives a predicted cross-front slope of 2.5×10^{-3}, vertical wavelength of 25 m, and growth rate of 2.5 days (Fig. 10). The growth predicted in the low-shear limit is significantly faster than the high-shear case. Including the horizontal density gradient increased the predicted cross-front slope and growth rate by 30% and 90% respectively. The effect on the vertical wavelength was smaller: an increase of roughly 15%.

The alongfront slope required in the low-shear limit is $2(\pm 1) \times 10^{-2}$, calculated from (33). With this alongfront slope, the relative rate of deformation by horizontal shear (i.e., $|\bar{v}_x|/\lambda$) is 2.5 ± 1.5 from (34). The rate of deformation by vertical shear [i.e., $|(l/m)\bar{v}_z|/\lambda$] is 1.1 ± 0.6 from (35). The shear rates and the predicted growth rate are of similar magnitude (Fig. 10). Therefore, it is not clear that the shear is either ''high'' or ''low.'' Perhaps the observed interleaving reflects an intermediate case.

d. Observed values

Ruddick (1992) estimated the density and salinity gradients along a number of interleaving layers. In the lower part of the meddy, he found the ratio of the along-layer gradients to be $\Delta\rho/\Delta S = 0.07(\pm 0.03)$ kg m^{-3} psu^{-1}. The cross-front and alongfront slopes of the layers are related to the observed ratio by

$$\frac{\Delta\rho}{\Delta S} = \frac{\bar{\rho}_x - [k/m + (l/m)\tan\phi]\bar{\rho}_z}{\bar{S}_x - [k/m + (l/m)\tan\phi]\bar{S}_z}, \qquad (50)$$

where ϕ is the angle of the ship's path relative to the front. Using (50), we estimate the slope of the layers along the transect $-[k/m + (l/m)\tan\phi] = 5.1(\pm 1.5) \times 10^{-3}$. If ϕ were zero, one could easily obtain the cross-front slope from this value. However, it is unlikely the transect was oriented directly across the front, so care must be taken while interpreting the observations.

In the high-shear limit, the interleaving layers do not slope along the front. Therefore, to evaluate the high-shear prediction, we set $l/m = 0$, which gives $-k/m = 5.1(\pm 1.5) \times 10^{-3}$. Comparing this value with the high-shear prediction yields good agreement (Fig. 10).

In the low-shear limit, the predicted alongfront slope ($-l/m$) is roughly 8 times the cross-front slope ($-k/m$). Taking this into account, and allowing a reasonable uncertainty in the orientation of the transect ($\phi = \pm 10°$), we are unable to estimate the cross-front slope or alongfront slope from the observed value.

From the spectrum shown in Ruddick and Hebert (1988), we estimate the most likely range of observed interleaving wavelengths to be $35(\pm 15)$ m. However, there appears to be an additional peak in the range $15(\pm 5)$ m. This could be an interleaving mode, but it might be an artifact of the processing (i.e., a harmonic of the main peak). Taking a cautious approach, we extend our range to include this second maximum (Fig. 10). The low-shear prediction agrees well with the observed wavelength. The high-shear prediction falls outside the observed range, but the uncertainties overlap. This suggests that the high-shear limit may not apply, but it is insufficient evidence to reject that limit outright.

From the analysis above, it is not clear which limit applies best to Meddy Sharon. In fact, the observed velocity fields suggest that the shear is intermediate, rather than ''high'' or ''low.'' This may be consistent with the rough overlap between observed values and the predictions of each limiting case.

7. Discussion

In this paper, we have investigated the behavior of double-diffusive interleaving in baroclinic fronts. An important outcome of the study is the prediction that interleaving layers will not slope in the alongfront direction if the background vertical or horizontal shear is strong. Comparing our high- and low-shear solutions, we have shown that the growth rate is significantly smaller in the high-shear case (Fig. 10). This suggests that double-diffusive interleaving may be diminished in fronts with strong baroclinic or barotropic shear.

In both the high- and low-shear limits, the strength of interleaving (i.e., the growth rate) is a function of the baroclinicity. Interleaving can be enhanced or suppressed, depending on the sign of the isopycnal slope (Figs. 7 and 9). Interleaving is enhanced if the isopycnals rise toward the fresh side of the front. Conversely, if the isopycnals slope downward across the front, the growth of interleaving is suppressed.

Previous studies have suggested that the driving force for double-diffusive interleaving is the cross-front gradient of salinity along isopycnal surfaces (McDougall 1985a; Ruddick 1992). While this holds in the absence of a horizontal density gradient, it is not true in baroclinic fronts. We have shown that interleaving is enhanced if the isopycnals rise toward the fresh side of the front (Figs. 7 and 9). However, with $\bar{S}_z > 0$, the cross-front gradient of salinity along isopycnals is diminished in this case. Therefore, we conclude that the salinity gradient along isopycnals is not a good indicator of expected interleaving strength.

The slope of interleaving layers relative to isopycnals is of interest because it affects directly the amount of diapycnal mixing generated by interleaving motions. It is often assumed that warm, salty fluid should rise relative to isopycnals if salt fingering is the driving mechanism. We have shown that this is not the case (Figs. 5 and 6). It is the layer slope relative to geopotential (i.e., horizontal) surfaces that determines the buoyancy

force along a layer. If salt fingering is the driving mechanism, warm salty fluid rises relative to surfaces of constant geopotential, but does not necessarily rise relative to surfaces of constant density.

Our analysis of Meddy Sharon highlighted a geometrical aspect of interleaving that must be taken into account when surveying ocean fronts. Because interleaving layers may slope to a much greater extent along fronts than across them, it is insufficient to survey only in the cross-front direction. Estimates of cross-front slope can easily be contaminated by the alongfront slope if the transect is not directly across the front. A minimum of two transects (one across and one along the front) are needed to adequately sample the three-dimensional structure of ocean interleaving.

In this study, we have investigated two limiting cases of double-diffusive interleaving. One limit is appropriate when the shear rate is high; the other when the background shear is low. This raises the question of how interleaving develops when the shear rate and the growth rate are roughly equal (e.g., Meddy Sharon). Do the interleaving layers simply remain unsloped along the front? Or, do they develop with the optimum alongfront slope and then flatten over time, twisting in the background shear? In the latter case, could shear provide a limiting mechanism, choking the growth of interleaving at finite amplitude?

Acknowledgments. We thank David Hebert, Barry Ruddick, and David Walsh for many interesting discussions on the dynamics of interleaving. We also thank the reviewers who provided many excellent suggestions for improvement of the manuscript. This work was supported by grants and scholarships from the Natural Sciences and Engineering Research Council of Canada and the Izaak Walton Killam Foundation.

REFERENCES

Armi, L., D. Hebert, N. Oakey, J. F. Price, P. L. Richardson, H. T. Rossby, and B. Ruddick, 1989: Two years in the life of a Mediterranean salt lens. *J. Phys. Oceanogr.,* **19,** 354–370.

Calman, J., 1977: Experiments on high Richardson number instability of a rotating stratified shear flow. *Dyn. Atmos. Oceans,* **1,** 277–297.

Emanuel, K. A., 1994: *Atmospheric Convection.* Oxford University Press, 392–412.

Hebert, D. L., 1988: A Mediterranean salt lens. Ph.D. thesis, Dalhousie University, 187 pp. [Available from Dalhousie University, Halifax, NS, B3H 4J1 Canada.]

——, N. Oakey, and B. Ruddick, 1990: Evolution of a Mediterranean salt lens: Scalar properties. *J. Phys. Oceanogr.,* **20,** 1468–1483.

Horne, E. P. W., 1978: Interleaving at the subsurface front in the slope water off Nova Scotia. *J. Geophys. Res.,* **83,** 3659–3671.

Joyce, T. M., W. Zenk, and J. M. Toole, 1978: The anatomy of the Antarctic Polar Front in the Drake Passage. *J. Geophys. Res.,* **83,** 6093–6113.

Kelley, D. E., 1990: Fluxes through diffusive staircases: A new formulation. *J. Geophys. Res.,* **95,** 3365–3371.

Kunze, E., 1990: The evolution of salt fingers in inertial wave shear. *J. Mar. Res.,* **48,** 471–504.

——, 1994: A proposed flux constraint for salt fingers in shear. *J. Mar. Res.,* **52,** 999–1016.

Kuzmina, N. P., and V. B. Rodionov, 1992: Influence of baroclinicity on formation of thermohaline intrusions in ocean frontal zones. *Izv. Atmos. Oceanic Phys.,* **28,** 804–810.

McDougall, T. J., 1985a: Double-diffusive interleaving. Part I: Linear stability analysis. *J. Phys. Oceanogr.,* **15,** 1532–1541.

——, 1985b: Double-diffusive interleaving. Part II: Finite amplitude, steady state interleaving. *J. Phys. Oceanogr.,* **15,** 1542–1556.

——, and B. R. Ruddick, 1992: The use of ocean microstructure to quantify both turbulent mixing and salt-fingering. *Deep-Sea Res.,* **39,** 1931–1952.

McIntyre, M. E., 1970: Diffusive destabilization of the baroclinic circular vortex. *Geophys. Fluid Dyn.,* **1,** 19–57.

Niino, H., 1986: A linear stability theory of double-diffusive horizontal intrusions in a temperature-salinity front. *J. Fluid Mech.,* **171,** 71–100.

Oakey, N. S., 1988: Estimates of mixing inferred from temperature and velocity microstructure. *Small-Scale Turbulence and Mixing in the Ocean,* J. C. J. Nihoul, and B. M. Jamart, Eds., Elsevier Science, 239–247.

Padman, L., 1994: Momentum fluxes through sheared oceanic thermohaline steps. *J. Geophys. Res.,* **99,** 10 799–10 806.

Ruddick, B., 1992: Intrusive mixing in a Mediterranean salt lens—Intrusion slopes and dynamical mechanisms. *J. Phys. Oceanogr.,* **22,** 1274–1285.

——, and J. S. Turner, 1979: The vertical length scale of double-diffusive intrusions. *Deep-Sea Res.,* **26A,** 903–913.

——, and D. Hebert, 1988: The mixing of Meddy ''Sharon.'' *Small-Scale Turbulence and Mixing in the Ocean,* J. C. J. Nihoul, and B. M. Jamart, Eds., Elsevier Science, 249–262.

——, R. W. Griffiths, and G. Symonds, 1989: Frictional stress at a sheared double-diffusive interface. *J. Geophys. Res.,* **94,** 18 161–18 173.

Schmitt, R. W., R. G. Lueck, and T. M. Joyce, 1986: Fine- and microstructure at the edge of a warm-core ring. *Deep-Sea Res.,* **33,** 1665–1689.

Stern, M. E., 1967: Lateral mixing of water masses. *Deep-Sea Res.,* **14,** 747–753.

Toole, J. M., and D. T. Georgi, 1981: On the dynamics and effects of double-diffusively driven intrusions. *Progress in Oceanography,* Vol. 10, Pergamon Press, 123–145.

Turner, J. S., 1973: *Buoyancy Effects in Fluids.* Cambridge University Press, 368 pp.

Walsh, D., and B. Ruddick, 1995: Double-diffusive interleaving: The influence of nonconstant diffusivities. *J. Phys. Oceanogr.,* **25,** 348–358.